Inorg. Chem. **2008**, *47*, 8343−8356

Behavior of BrO_3F and ClO_3F Toward Strong Lewis Acids and the Characterization of $[XO_2][SbF_6]$ (X = Cl, Br) by Single Crystal X-ray Diffraction, Raman Spectroscopy, and Computational Methods

John F. Lehmann,[†] Sebastian Riedel, and Gary J. Schrobilgen*

Department of Chemistry, McMaster University, Hamilton, Ontario L8S 4M1, Canada

Received May 21, 2008

The interactions of BrO_3F and ClO_3F with the strong Lewis acids AsF_5 and SbF_5 were investigated. Although ClO_3F is unreactive toward AsF_5 and SbF_5, BrO_3F undergoes fluoride ion abstraction and O_2 elimination, accompanied by central halogen reduction, to form $[BrO_2][Sb_nF_{5n+1}]$ ($n \geq 1$), rather than simple fluoride ion abstraction to form BrO_3^+ salts. The geometric parameters of the BrO_2^+ cation have been obtained in the solid state for the first time by a single-crystal X-ray diffraction study of $[BrO_2][SbF_6]$ at −173 °C and are compared with those of ClO_2^+ salts. Quantum-chemical calculations have been used to arrive at the geometries and vibrational frequencies of XO_2^+ and XO_3^+ (X = Cl, Br) and have been compared with the experimental values for XO_2^+. The calculations have also been used to account for the contrasting behaviors of ClO_3F and BrO_3F toward central halogen reduction in the presence of liquid SbF_5. The thermochemical stabilities of ClO_3^+ and BrO_3^+ salts of the AsF_6^-, SbF_6^-, $Sb_2F_{11}^-$, and $Sb_3F_{16}^-$ were also investigated, which provided the fluoride ion affinities of AsF_5, SbF_5, Sb_2F_{10}, and Sb_3F_{15} up to and including the CCSD(T) level of theory. These values are compared with the current literature values. Thermochemical studies indicate that XO_3^+ formation by fluoride ion abstraction from XO_3F is not spontaneous under standard conditions whereas a concerted fluoride abstraction and O_2 elimination to give the XO_2^+ cations is spontaneous to near thermally neutral. Failure to observe reactivity between ClO_3F and any of the aforementioned Lewis acid fluoride ion acceptors is attributed to a significant kinetic barrier to fluoride ion abstraction.

Introduction

The fluoride ion donor and acceptor properties of the fluorides and oxide fluorides of bromine and chlorine in the III and V oxidation states have been investigated in detail and have permitted the isolation of salts containing cations and anions derived from ClF_3 (ClF_2^+,[1,2] ClF_4^- [3]), BrF_3 (BrF_2^+,[4] BrF_4^-[5,6]), ClF_5 (ClF_4^+,[7] ClF_6^-[8,9]), BrF_5 (BrF_4^+,[7,10] BrF_6^-[9,11–13]), ClO_2F (ClO_2^+,[14–22] $ClO_2F_2^-$ [23]), BrO_2F (BrO_2^+,[24–26] $BrO_2F_2^-$[26,27]), $ClOF_3$ ($ClOF_2^+$,[28,29] $ClOF_4^-$[28,30]),

* To whom correspondence should be addressed. E-mail: schrobil@mcmaster.ca.

† Present address: Air Products and Chemicals, Inc., 7201 Hamilton Blvd., Trexlertown, PA 18195.

(1) Bougon, R.; Cicha, W. V.; Lance, M.; Meublat, L.; Nierlich, M.; Vigner, J. *Inorg. Chem.* **1991**, *30*, 102–109.
(2) Antipin, M. Yu.; Ellern, A. M.; Sukhoverkhov, V. F.; Struchkov, Yu. T.; Buslaev, Yu. A. *Russ. J. Inorg. Chem.* **1988**, *33*, 171–173; *Zh. Neorg. Khim.* **1988**, *33*, 307−311.
(3) Zhang, X.; Seppelt, K. *Z. Anorg. Allg. Chem.* **1997**, *623*, 491–500.
(4) Edwards, A. J.; Christe, K. O. *J. Chem. Soc., Dalton Trans.* **1976**, 175–1777.
(5) Wilson, W. W.; Christe, K. O. *Inorg. Chem.* **1989**, *28*, 4172–4175.
(6) Christe, K. O.; Wilson, W. W. *Inorg. Chem.* **1986**, *25*, 1904–1906.
(7) Christe, K. O.; Zhang, X.; Sheehy, J. A.; Bau, R. *J. Am. Chem. Soc.* **2001**, *123*, 6338–6348.
(8) Christe, K. O.; Wilson, W. W.; Chirakal, R. V.; Sanders, J. C. P.; Schrobilgen, G. J. *Inorg. Chem.* **1990**, *29*, 3506–3511.
(9) Dixon, D. A.; Grant, D. J.; Christe, K. O.; Peterson; K. A. *Inorg. Chem.* **2008**, *47*, 5485–5494.
(10) Vij, A.; Tham.Fook, S.; Vij, V.; Wilson, W. W.; Christe, K. O. *Inorg. Chem.* **2002**, *41*, 6397–6403.
(11) Mahjoub, A. R.; Zhang, X.; Seppelt, K. *Chem.—Eur. J.* **1995**, *1*, 261–265.
(12) Mahjoub, A. R.; Hoser, A.; Fuchs, J.; Seppelt, K. *Angew.Chem., Int. Ed. Engl.* **1989**, *28*, 1526–1527; *Angew. Chem., Int. Ed. Engl.* **1989**, *101*, 1528−1529.
(13) Christe, K. O.; Wilson, W. W. *Inorg. Chem.* **1989**, *28*, 3275–3277.
(14) Nabiev, S. S. *Russ Chem. Bull.* **1999**, *48*, 711–717.
(15) Christe, K. O. *Inorg. Chem.* **1973**, *12*, 1580–1587.
(16) Schmeisser, M.; Brändle, K. *Adv. Inorg. Chem. Radiochem.* **1963**, *5*, 41–89.
(17) Christe, K. O.; Schack, C. J.; Pilipovich, D.; Sawodny, W. *Inorg. Chem.* **1969**, *8*, 2489–2494.
(18) Tobias, K. M.; Jansen, M. *Z. Anorg. Allg. Chem.* **1987**, *550*, 16–26.
(19) Edwards, A. J.; Sills, R. J. C. *J. Chem. Soc., Dalton Trans.* **1974**, 1726–1729.
(20) Antipin, M. Y.; Ellern, A. M.; Sukhoverkhov, V. F.; Struchkov, Yu. T.; Buslaev, Yu. A. *Dokl. Akad. Nauk SSSR* **1987**, *293*, 1152–1155; *Dokl. Akad. SSSR, Engl.* **1987**, *293*, 354.

10.1021/ic800929h CCC: $40.75
Published on Web 08/14/2008

and $BrOF_3$ ($BrOF_2^+$,[26,31,32] $BrOF_4^-$[26,33]). In contrast with the rich fluoride ion transfer chemistry of the III and V oxidation states, fluoride ion transfer reactions involving Br(VII) and Cl(VII) species are relatively rare and have only been established by the syntheses of $BrO_3F_2^-$[34] (eq 1) and ClO_2F_3[35,36] (eq 2).

$$BrO_3F + F^- \rightarrow BrO_3F_2^- \quad (1)$$

$$ClO_2F_2^+ + F^- \rightarrow ClO_2F_3 \quad (2)$$

The exploitation of similar Lewis acid−base reactions for the preparation of new Br(VII) and Cl(VII) cations and anions is complicated by several factors, including the stronger ligand−ligand repulsions encountered for the high-coordination-number neutral and anionic halogen(VII) oxide fluorides[37] and the inability to prepare their neutral precursors $ClOF_5$,[38] $BrOF_5$,[26,39] and BrO_2F_3.[26] Perbromyl fluoride[26] and ClO_3F[40,41] fail to exhibit fluoride ion donor properties toward the strong Lewis acids AsF_5 and SbF_5 in anhydrous HF (aHF), preventing the isolation of salts containing the BrO_3^+ and ClO_3^+ cations from this medium. The cations, however, have been observed as stable ions in the mass spectra of BrO_3F[42] and ClO_3F.[43]

In contrast, BrO_2F and ClO_2F are well documented fluoride ion bases and readily react with fluoride ion acceptors to form BrO_2^+ and ClO_2^+ salts. The vibrational spectra of ClO_2^+[14−18] and BrO_2^+[24−26] have been reported previously and are consistent with the bent geometry predicted by the VSEPR[44] model. Single-crystal X-ray diffraction has been used to obtain accurate geometric parameters for the ClO_2^+ cation in its $Sb_2F_{11}^-$,[19] BF_4^-,[20,21] GeF_5^-,[21] ClO_4^-,[18] and RuF_6^-[22] salts; however, the geometry of BrO_2^+ has only been estimated from the photoelectron spectrum of the BrO_2• radical using an iterative Franck−Condon analysis.[45,46] Modern computational methods have been used to investigate the structure and vibrational frequencies of BrO_2^+[45,47] but have not been employed for the characterization of ClO_2^+.

In the present study, the reactions of BrO_3F and ClO_3F with liquid SbF_5 were investigated with the anticipation that this highly acidic medium might yield BrO_3^+ and/or ClO_3^+ salts. In the course of this study, the crystal structures of $[BrO_2][SbF_6]$ and $[ClO_2][SbF_6]$ were determined by low-temperature single-crystal X-ray diffraction. Quantum-chemical calculations have been used to corroborate experimental geometries and vibrational frequencies of ClO_2^+ and BrO_2^+, to arrive at the predicted counterparts for ClO_3^+ and BrO_3^+, and to address the underlying thermochemistries of these systems.

Results and Discussion

Reactions of BrO_3F with SbF_5 and AsF_5. The reaction of BrO_3F with SbF_5 proceeded vigorously at 0 °C with the evolution of O_2 and the formation of a red-orange solid, which was identified by Raman spectroscopy as $[BrO_2][Sb_nF_{5n+1}]$ ($n \geq 1$) from the intense BrO_2 stretching modes of the bromyl cation at 870 and 937 cm^{-1}.[24] Other oxygen-containing bromine species were not observed in the Raman spectrum of the product, suggesting that the reaction proceeds quantitatively according to eq 3.

$$BrO_3F + nSbF_5 \xrightarrow{SbF_5,\ 0\ ^\circ C} [BrO_2][Sb_nF_{5n+1}] + {}^1/_2O_2 \quad (3)$$

A similar reaction does not occur at −78 °C when neat AsF_5 is used in place of SbF_5; however, $[BrO_2][Sb_nF_{5n+1}]$ can be synthesized in this manner at temperatures as low as −45 °C if excess SbF_5 is dissolved in AsF_5, indicating that the stronger Lewis acids, $(SbF_5)_n$ ($n > 1$), are required to initiate the reaction. Red-orange $[BrO_2][SbF_6]$ was obtained by recrystallization of $[BrO_2][Sb_nF_{5n+1}]$ from aHF, and the purity of the salt was ascertained by low-temperature Raman spectroscopy.

Reactions of ClO_3F and ClO_2F with SbF_5. Perchloryl fluoride failed to react with liquid SbF_5 at temperatures as high as 20 °C, which is consistent with previous reports that ClO_3F does not form adducts with BF_3, PF_5, AsF_5, SbF_5, and SO_3.[40] The chloryl salt, $[ClO_2][SbF_6]$, was prepared by the reaction of ClO_2F with SbF_5 in aHF (eq 4), and was isolated in high purity by recrystallization from aHF.

$$ClO_2F + SbF_5 \xrightarrow{HF} [ClO_2][SbF_6] \quad (4)$$

Crystal Structures of $[XO_2][SbF_6]$ (X = Cl, Br). The unit cell parameters and refinement statistics for the $[XO_2][SbF_6]$ salts are summarized in Table 1 and the relevant geometric parameters are provided in Table 2. Both salts crystallize in the monoclinic space group *P2/c* and are

(21) Mallouk, T. E.; Rosenthal, G. L.; Müller, G.; Brusasco, R.; Bartlett, N. *Inorg. Chem.* **1984**, *23*, 3167–3173.
(22) Bougon, R.; Cicha, W. V.; Lance, M.; Meublat, L.; Nierlich, M.; Vigner, J. *Inorg. Chem.* **1991**, *30*, 102–109.
(23) Christe, K. O.; Curtis, E. C. *Inorg. Chem.* **1972**, *11*, 35–39.
(24) Jacob, E. *Angew. Chem., Int. Ed. Engl.* **1976**, *15*, 158; *Angew. Chem.* **1976**, *88*, 189−190.
(25) Spekkens, P. H. McMaster University, Hamilton, ON, Canada, 1977.
(26) Gillespie, R. J.; Spekkens, P. H. *Isr. J. Chem.* **1978**, *17*, 11–19.
(27) Gillespie, R. J.; Spekkens, P. H. *J. Chem. Soc., Dalton Trans.* **1976**, 2391–2396.
(28) Christe, K. O.; Schack, C. J.; Pilipovich, D. *Inorg. Chem.* **1972**, *11*, 2201–2205.
(29) Christe, K. O.; Curtis, E. C.; Schack, C. J. *Inorg. Chem.* **1972**, *11*, 2212–2215.
(30) Christe, K. O.; Curtis, E. C. *Inorg. Chem.* **1972**, *11*, 2209–2211.
(31) Adelhelm, M.; Jacob, E. *Angew. Chem., Int. Ed. Engl.* **1977**, *16*, 461; *Angew. Chem.* **1977**, *89*, 476−477.
(32) Bougon, R.; Huy, T. B.; Charpin, P.; Gillespie, R. J.; Spekkens, P. H. *J. Chem. Soc., Dalton Trans.* **1979**, 6–12.
(33) Ellern, A.; Boatz, J. A.; Christe, K. O.; Drews, T.; Seppelt, K. *Z. Anorg. Allg. Chem.* **2002**, *628*, 1991–1999.
(34) Lehmann, J. F.; Schrobilgen, G. J. *J. Am. Chem. Soc.* **2005**, *127*, 9416–9427.
(35) Christe, K. O.; Wilson, R. D. *Inorg. Chem.* **1973**, *12*, 1356–1357.
(36) Christe, K. O.; Curtis, E. C. *Inorg. Chem.* **1973**, *12*, 2245–2251.
(37) Robinson, E. A.; Gillespie, R. J. *Inorg. Chem.* **2003**, *42*, 3865–3872.
(38) Schack, C. J.; Lindahl, C. B.; Pilipovich, D.; Christe, K. O. *Inorg. Chem.* **1972**, *11*, 2201–2205.
(39) Pilipovich, D.; Rogers, H. H.; Wilson, R. D. *Inorg. Chem.* **1972**, *11*, 2192–2195.
(40) Christe, K. O.; Schack, C. J. *Adv. Inorg. Chem. Radiochem.* **1976**, *18*, 319–398.
(41) Wamser, C. A.; Fox, W. B.; Gould, D.; Sukornick, B. *Inorg. Chem.* **1968**, *7*, 1933–1935.
(42) Appleman, E. H.; Studier, M. H. *J. Am. Chem. Soc.* **1969**, *91*, 4561–4562.
(43) Alekseev, V. I.; Fedorova, L. I.; Baluev, A. V. *Russ. Chem. Bull.* **1983**, *32*, 980–986.

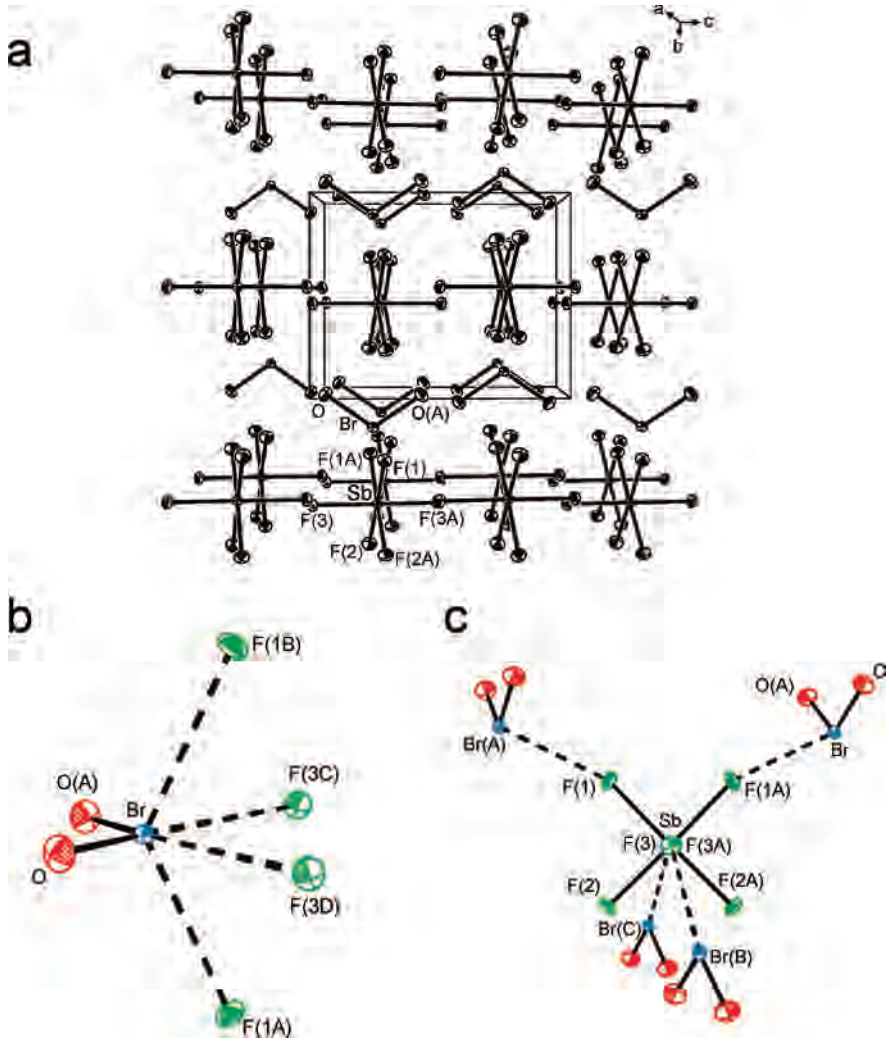

Figure 1. Crystal structure of $[BrO_2][SbF_6]$ at −173 °C. (a) Packing diagram viewed along the *a*-axis, and close contacts around (b) the BrO_2^+ cation and (c) the SbF_6^- anion. Thermal ellipsoids are shown at the 50% probability level.

isostructural and isomorphous with $[ClO_2][RuF_6]$.[22] The unit cell symmetry constrains the site symmetries of the cations and anions to C_2, resulting in one crystallographically unique X−O bond and three unique Sb−F bonds.

The packing is best described in terms of alternating layers of cations and anions lying parallel to the *ac*-plane (Figures 1a and 2a). The XO_2^+ and SbF_6^- ions are coplanar in the *ab*-plane but are staggered along the *bc*-plane such that each cation has four long cation−anion X- - -F contacts lying within the sum of the van der Waals radii[48] of Br (1.85 Å), Cl (1.75 Å), and F (1.47 Å) (Figures 1b and 2b). The XO_2^+ cations are oriented such that the X−E axis (E = lone pair) bisects the angles subtended by the X- - -F contacts (i.e., F(1A)- - -X- - -F(1B), F(3C)- - -X- - -F(3D)). The structurally equivalent X- - -F(1A) and X- - -F(3C) cation−anion contact distances in $[BrO_2][SbF_6]$ (2.590(1), 2.685(1) Å) and $[ClO_2][SbF_6]$ (2.517(4), 2.738(4) Å) differ significantly but have similar average values (Br, 2.64(5) Å; Cl, 2.63(11) Å) despite the large covalent radius difference for chlorine and bromine. This, along with the similar average Cl- - -F distances for $[ClO_2][RuF_6]$ (2.61(12) Å),[22] $[ClO_2][Sb_2F_{11}]$ (2.68(7) Å),[19] and $[ClO_2][BF_4]$ (2.60(5),[20] 2.64(4)[21] Å) and the average Cl−O distance for $[ClO_2][ClO_4]$ (2.67(9) Å),[18] suggests that these contact distances are not coincidental but play an important role in orientating the comparatively small XO_2^+ cations within their large interstitial anion cavities. Correspondingly, four secondary bonding interactions occur between each anion and four different cations, consisting of two *trans*- and two *cis*-contacts with the anion (Figure 1c).

The Br−O bonds of $[BrO_2][SbF_6]$ (1.595(2) Å) are shorter but comparable to the bond length estimated for the gas-phase BrO_2^+ cation (1.6135 Å) from the photoelectron spectrum of the $BrO_2\cdot$ radical.[45] The bond lengths of the BrO_2^+ cation are similar to those of the Br(V)−O bonds in $[NO_2][BrF_4]\cdot 2BrOF_3$ (1.569, 1.606 Å)[49] and $[NO][BrOF_4]$ (1.575(3) Å)[49] and the terminal Br−O bonds in $O_2BrOBrO_2$

(44) Gillespie, R. J.; Hargittai, I. *The VSEPR Model of Molecular Geometry*; Allyn and Bacon: Boston, 1991.
(45) Dyke, J. M.; Gamblin, S. D.; Hooper, N.; Lee, E. P. F.; Morris, A.; Mok, D. K. W.; Chau, F. T. *J. Chem. Phys.* **2000**, *112*, 6262–6274.
(46) Chau, F. T.; Dyke, J. M.; Lee, E. P.-f.; Wang, D.-c. *J. Electron Spectrosc. Relat. Phenom.* **1998**, *97*, 33–47.
(47) Francisco, J. S. *Chem. Phys. Lett.* **1998**, *288*, 307–310.
(48) Bondi, A. *J. Phys. Chem.* **1964**, *68*, 441–451.
(49) Ellern, A.; Boatz, J. A.; Christe, K. O.; Drews, T.; Seppelt, K. *Z. Anorg. Allg. Chem.* **2002**, *628*, 1991–1999.

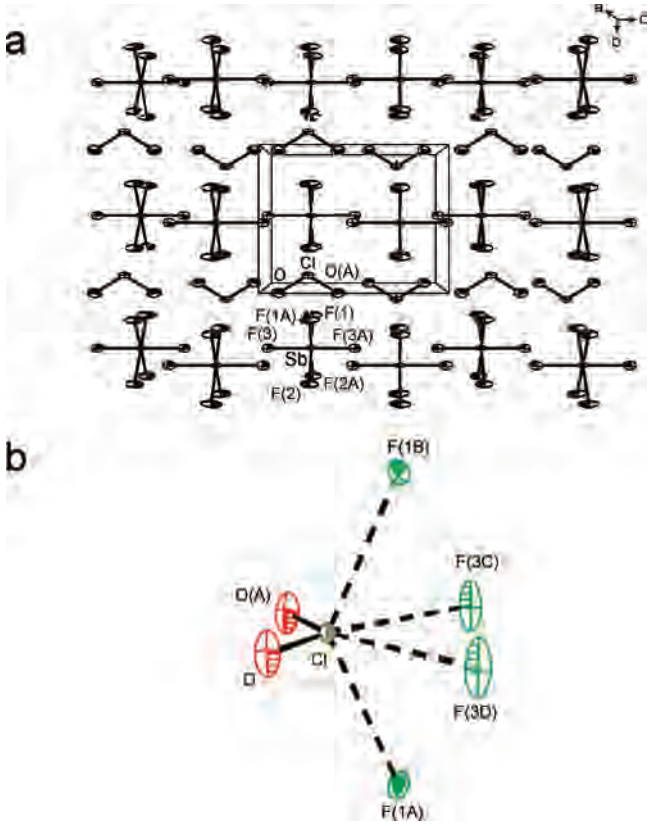

Figure 2. Crystal structure of $[ClO_2][SbF_6]$ at −173 °C. (a) Packing diagram viewed along the *a*-axis and (b) close contacts around the ClO_2^+ cation. The anion coordination in $[ClO_2][SbF_6]$ is very similar to that in $[BrO_2][SbF_6]$ (see Figure 1b). Thermal ellipsoids are shown at the 50% probability level.

(1.606(12), 1.611(2), 1.613(2), 1.606(2) Å)[50] and $O_2BrOTeF_5$ (1.595(4), 1.608(3) Å).[51] Unfortunately, comparisons among the bond lengths of the cation and its parent oxide fluoride, BrO_2F, cannot be made because the crystal structure of BrO_2F is disordered.[51] The Br−O bonds in these species are shorter than those of BrO_3^- (1.648(4) Å)[52] and the structurally related BrO_2• radical (1.6491(15) Å)[53] but are comparable to that reported for the $BrOF_4^-$ anion (1.575(3) Å).[49]

The Cl−O bond lengths in $[ClO_2][SbF_6]$ (1.385(5) Å) are equal, within $\pm 3\sigma$, to those determined for ClO_2^+ in the RuF_6^- salt (1.379(9) Å)[22] but shorter than those of the BF_4^- (1.405(1), 1.408(1);[20] 1.397(2), 1.390(2)[21] Å) and ClO_4^- (1.406(2), 1.410(2) Å)[18] salts. It is not possible to make a valid comparison with the Cl−O bond lengths of the $Sb_2F_{11}^-$ (1.28(3), 1.31(4) Å)[19] salt owing to the low precision of this structure; however, within $\pm 2\sigma$, the Cl−O bond lengths contract, with decreasing anion charge density. The trend reflects a reduction in electron density transfer from the anion to the cation via secondary bonding interactions as the anion basicity decreases. Although the $[ClO_2][BF_4]$ and $[ClO_2][ClO_4]$ salts provide the longest Cl−O bond lengths, they are still significantly shorter than those of the ClO_2• radical (1.475(3) Å).[54] Overall, the ClO_2^+ bond lengths are similar to the Cl(V)−O bond lengths of gaseous ClO_2F (1.419(9) Å)[55] and $ClOF_3$ (1.405(3)[56] but are significantly shorter than those of ClO_3^- (1.502(3) Å),[57] in accord with the lower formal Cl−O bond order of the anion ($^5/_3$) and the trends noted for the Br(V) analogues.

The O−Br−O bond angle in $[BrO_2][SbF_6]$ (111.9(1)°) is significantly smaller than the O−Cl−O bond angles determined in the structures of $[ClO_2][SbF_6]$ (117.8(4)°), $[ClO_2][RuF_6]$ (117.2(9)°),[22] $[ClO_2][ClO_4]$ (118.9(2)°),[18] $[ClO_2][BF_4]$ (118.47(6)°,[20] 119.0(1)°[21]), and $[ClO_2][Sb_2F_{11}]$ (122(2)°).[19] The bond angles of both XO_2^+ cations are consistent with the

Table 1. Summary of Crystal Data and Refinement Results for $[BrO_2][SbF_6]$ and $[ClO_2][SbF_6]$

	$[BrO_2][SbF_6]$	$[ClO_2][SbF_6]$
space group	*P2/c*	*P2/c*
a (Å)	7.251(2)	7.194(1)
b (Å)	5.779(1)	5.682(1)
c (Å)	10.045(2)	10.225(2)
β (deg)	133.23(3)	134.68(3)
V (Å^3)	306.7(2)	297.1(3)
Z	2	2
mol. mass (g mol^{-1})	347.63	303.18
ρ_{calcd} (g cm^{-3})	3.765	3.389
T (°C)	−173	−173
μ (mm^{-1})	11.08	5.16
R_1[a]	0.0129	0.0527
wR_2[a]	0.0328	0.1144

[a] R_1 is defined as $\sum||F_o| - |F_c||/\sum|F_o|$ for $I > 2\sigma(I)$; wR_2 is defined as $[\sum[w(F_o^2 - F_c^2)^2]/\sum w(F_o^2)^2]^{1/2}$ for $I > 2\sigma(I)$.

Table 2. Bond Lengths and Bond Angles for $[XO_2][SbF_6]$ (X = Br, Cl)

	$[BrO_2][SbF_6]$	$[ClO_2][SbF_6]$
	Bond Lengths (Å)	
X−O	1.595(2)	1.385(5)
Sb−F(1)	1.884(2)	1.880(3)
Sb−F(2)	1.888(1)	1.870(3)
Sb−F(3)	1.869(1)	1.864(5)
X- - -F(1A)	2.590(1)	2.517(4)
X- - -F(3C)	2.685(1)	2.738(4)
	Bond Angles (deg)	
O−X−O(A)	111.9(1)	117.8(4)
F(1)−Sb−F(2)	90.04(5)	91.4(2)
F(1)−Sb−F(3)	90.85(5)	89.5(2)
F(2)−Sb−F(3)	90.46(6)	89.5(2)
O- - -X- - -F(1A)	101.30(7)	102.2(3)
O- - -X- - -F(1B)	105.88(7)	102.0(3)
O- - -X- - -F(3C)	81.49(6)	80.8(2)
O- - -X- - -F(3D)	166.44(6)	161.4(2)
O(A)- - -X- - -F(1A)	105.88(7)	102.0(3)
O(A)- - -X- - -F(1B)	101.30(7)	102.2(3)
O(A)- - -X- - -F(3C)	166.44(6)	161.4(2)
O(A)- - -X- - -F(3D)	81.49(6)	80.8(2)
F(1A)- - -X- - -F(1B)	130.48(6)	132.3(2)
F(1A)- - -X- - -F(3C)	72.37(5)	72.2(2)
F(1A)- - -X- - -F(3D)	71.71(4)	71.9(2)
F(3C)- - -X- - -F(3D)	85.30(6)	80.6(2)
F(1B)- - -X- - -F(3D)	72.37(5)	72.2(2)

(50) Leopold, D.; Seppelt, K. *Angew. Chem., Int. Ed. Engl.* **1994**, *33*, 975–976; *Angew. Chem.* **1994**, *106*, 1043−1044.
(51) Hwang, I.-C.; Kuschel, R.; Seppelt, K. *Z. Anorg. Allg. Chem.* **1997**, *623*, 379–383.
(52) Abrahams, S. C.; Bernstein, J. L. *Acta Crystallogr., Sect. B* **1977**, *33*, 3601–3604.
(53) Müller, H. S. P.; Miller, C. E.; Cohen, E. A. *Angew. Chem., Int. Ed. Engl.* **1996**, *35*, 2129–2131; *Angew. Chem.* **1996**, *108*, 2285−228.
(54) Tobias, K. M.; Jansen, M. *Angew. Chem., Int. Ed. Engl.* **1986**, *25*, 993–994; *Angew. Chem.* **1986**, *98*, 994−995.
(55) Robiette, A. G.; Parent, C. R.; Gerry, M. C. L. *J. Mol. Spectrosc.* **1981**, *86*, 455–464.
(56) Oberhammer, H.; Christe, K. O. *Inorg. Chem.* **1982**, *21*, 273–275.
(57) Burke-Laing, M. E.; Trueblood, K. N. *Acta Crystallogr., Sect. B* **1977**, *33*, 2698–2699.
(58) Pople, J. A.; Scott, A. P.; Wong, M. W.; Radom, L. *Isr. J. Chem.* **1993**, *33*, 345–350.

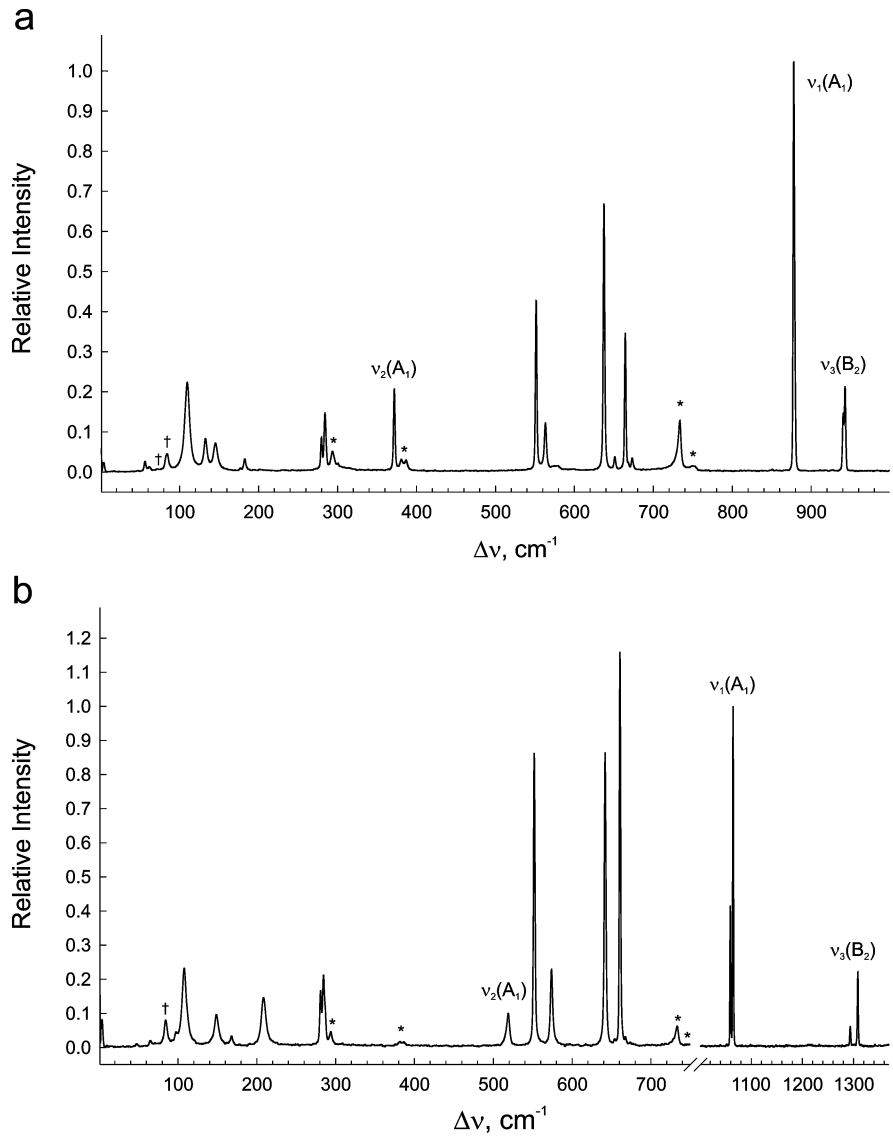

Figure 3. Raman spectra of crystalline (a) $[BrO_2][SbF_6]$ and (b) $[ClO_2][SbF_6]$. The spectra were recorded at −163 °C using 1064-nm excitation. The bands labeled $\nu_1(A_1)$, $\nu_2(A_1)$, and $\nu_3(B_2)$ are assigned to the XO_2^+ cations (Table 3). Unlabeled bands arise from the SbF_6^- anion (Table 3). Bands arising from the FEP sample tube are denoted by asterisks (*) and daggers (†) denote laser artifacts.

VSEPR model, which predicts a trigonal-planar AX_2E arrangement, having an O−X−O bond angle slightly less than 120° on account of the larger electron lone pair domain when compared with the more localized bonding pairs. On the basis of the narrow range of bond angles obtained for the ClO_2^+ salts and the similar bond angles obtained for the gaseous BrO_2· (114.44(25)°)[53] and ClO_2· (117.7(1.7)°)[53] radicals, the interionic contacts observed in the crystal structures of the XO_2^+ salts (vide supra) do not appear to have a strong influence on the O−X−O bond angles.

Vibrational Spectra of $[XO_2][SbF_6]$ (X = Cl, Br). The vibrational frequencies of $[BrO_2][SbF_6]$ and $[ClO_2][SbF_6]$ obtained from Raman spectroscopy (Figure 3) are summarized in Table 3, and those previously reported for $[BrO_2][Sb_{2.24}F_{12.2}]$,[24] $[BrO_2][AsF_6]$,[25,26] $[BrO_2][BF_4]$,[25,26] $[ClO_2][MF_6]$ (M = As,[17] Ru,[22] Pt,[15] Ir,[15] Au[14]), $[ClO_2][BF_4]$,[17] and $[ClO_2][ClO_4]$[18] are listed in the Supporting Information, Tables S1 (BrO_2^+) and S2 (ClO_2^+). Vibrational frequency assignments of the XO_2^+ cations are in agreement with previous assignments and with quantum-chemical calculations (Table 3; also see Computational Results).

The three fundamental vibrations ($\Gamma_{vib} = 2A_1 + B_2$) of the BrO_2^+ and ClO_2^+ cations exhibit anion dependencies, which are greatest for $\nu_1(A_1)$ (Br, 862−884; Cl, 1039−1065 cm^{-1}) and $\nu_3(B_2)$ (Br, 931−947; Cl, 1280−1308 cm^{-1}) and least for $\nu_2(A_1)$ (Br, 372−382; Cl, 518−521 cm^{-1}). These anion-dependent shifts do not correlate with the size or fluoride ion basicity of the anion; however, the similar frequency shifts observed among the chlorine and bromine analogues of the $[XO_2][SbF_6]$ and $[XO_2][AsF_6]$ salts imply that they are likely related to the cation−anion packing arrangements and long X−F contacts within their crystal lattices.

The Raman spectra of both $[XO_2][SbF_6]$ salts exhibit split cation and anion bands. In order to account for these splittings, factor-group analyses have been carried out based on the crystal structure determinations of the isomorphous $[XO_2][SbF_6]$ salts (Supporting Information, Table S3).

Table 3. Experimental and Calculated Vibrational Frequencies[a] for $[XO_2][SbF_6]$ (X = Br, Cl)

assgnt[b]		exptl[c]	HF[d,e]	MP2[d] 6-311G(d)	QCISD[d] 6-311G(2d)	CCSD(T)[f] aug-cc-pVTZ	MPW1PW91[d] DZVP	B3LYP[d,f] aug-cc-pVQZ
				BrO_2^+				
$\nu_1(A_1)$, $\nu_s(BrO_2)$	^{79}Br	877.9(100)	999(82)[3]	844.0(5198)[2]	865.7[2]	844.7	939.6(30)[<1]	941.8(32)[<1]
	^{81}Br				864.5[2]			
$\nu_2(A_1)$, $\delta(OBrO)$	^{79}Br	371.9(21)	388(3)[35]	325.9(13)[10]	349.6[13]	337.9	348.7(4)[14]	361.8(3)[13]
	^{81}Br				348.8[13]			
$\nu_3(B_2)$, $\nu_{as}(BrO_2)$	^{79}Br	942.8(21)	1096(15)[57]	1072.9(279)[758]	968.4[21]	930.3	1016.4(10)[28]	1016.8(8)[22]
	^{81}Br	940.5(15)			965.6[20]			
				ClO_2^+				
$\nu_1(A_1)$, $\nu_s(ClO_2)$	^{35}Cl	1064.7(100)	1176(70)[18]	901.4(1823)[<1]	1019.5[3]	986.1	1097.7(28)[5]	1100.2(30)[5]
	^{37}Cl	1059.4(42)			1014.0[3]			
$\nu_2(A_1)$, $\delta(OBrO)$	^{35}Cl	518.9(10)	610.0(3)[54]	446.9(2)[20]	503.7[22]	484.2	503.1(4)[27]	517.3(2)[20.6]
	^{37}Cl				499.9[21]			
$\nu_3(B_2)$, $\nu_{as}(BrO_2)$	^{35}Cl	1308.3(22)	1597.4(12)[139]	1173.1(22)[136]	1290.4[53]	1237.3	1340.4(9)[71]	1347.4(15)[64]
	^{37}Cl	1293.5(6)			1276.1[50]			

assgnt (O_h)	SbF_6^- in $[BrO_2][SbF_6]$[c]	SbF_6^- in $[ClO_2][SbF_6]$[c]
$\nu_1(A_{1g})$	664.5(35)	660.7(116)
$\nu_2(E_g)$	563.4(12) 551.1(43)	573.8(22) 551.9(86)
$\nu_3(T_{1u})$	673.2(3) 651.1(4) 637.7(67)	667.9(3) 653.9(2) 641.9(86)
$\nu_5(T_{2g})$	284.2(15) 279.7(8)	284.6(21) 280.9(16)
$\nu_6(T_{2u})$	145.3(8)[g]	148.7(9)[g]

[a] Frequencies are given in cm^{-1}. [b] Symbols denote symmetric stretch (ν_s), asymmetric stretch (ν_{as}), and bend (δ). [c] Relative intensities are given in parentheses. In addition to the modes listed above, several low-frequency modes were observed for $[BrO_2][SbF_6]$ (182.4(4), 132.7(9), 109.6(23), 61.4(1), 55.1(3) cm^{-1}) and $[ClO_2][SbF_6]$ (208.5(15), 167.9(3), 107.8(24), 96.1 (sh), 65.1(2) cm^{-1}) that arise from the X—F contact interactions with the SbF_6^- anions (also see discussion and in Supporting Information, Tables S4 and S5). [d] Calculated Raman intensities ($Å^4$ amu^{-1}) are given in parentheses and calculated infrared intensities (km mol^{-1}) are given in square brackets. [e] Scaled by 0.8953 as recommended in ref 58. [f] Frequencies were calculated using the average mass. [g] Tentative assignment.

Under the unit cell symmetry, C_{2h}, the $\nu_1(A_1)$ and $\nu_2(A_1)$ bands of the free cation (C_{2v} symmetry) are each split into an A_g and an A_u component, whereas the $\nu_3(B_2)$ mode is split into a B_g and a B_u component. The factor-group analysis does not, however, account for the splittings observed in the Raman spectra because the A_u and B_u components are formally Raman inactive under the centrosymmetric unit cell symmetry, C_{2h}. Rather, the cation band splittings are attributable to isotope shifts arising from the two naturally occurring isotopes of bromine (^{79}Br, 50.7%; ^{81}Br, 49.3%) and chlorine (^{35}Cl, 75.8%; ^{37}Cl, 24.2%). This explanation is consistent with the similar peak heights of the split $\nu_3(B_2)$ band of $[BrO_2][SbF_6]$, and the ~3:1 peak height ratios observed for the split $\nu_1(A_1)$ and $\nu_3(B_2)$ bands of many ClO_2^+ salts (Supporting Information, Table S2), where the more intense band is always higher in frequency and is assigned to $^{35}ClO_2^+$. The larger isotopic splittings observed for $[ClO_2][SbF_6]$ ($\Delta\nu_1 = 5.3$ cm^{-1}; $\Delta\nu_3 = 14.8$ cm^{-1}) when compared with $[BrO_2][SbF_6]$ ($\Delta\nu_3 = 2.3$ cm^{-1}) are in excellent agreement with the isotopic splittings calculated for the gas-phase ClO_2^+ ($\Delta\nu_1 = 5.5$ cm^{-1}; $\Delta\nu_3 = 14.3$ cm^{-1}) and BrO_2^+ ($\Delta\nu_1 = 1.2$ cm^{-1}; $\Delta\nu_3 = 2.8$ cm^{-1}) cations by use of the QCISD method (see Table 3) and reflect the greater difference in reduced masses for the chlorine isotopes.

In contrast, the anion splittings are accounted for in the factor-group analysis of the SbF_6^- anion (Supporting Information, Table S3), which predicts each of the Raman-active bands under O_h symmetry to be split into Raman-active g-components and infrared-active u-components under C_{2h} symmetry of the unit cell (given in square brackets): $\nu_1(A_{1g})$ [$A_g + A_u$], $\nu_2(E_g)$ [$2A_g + 2A_u$], and $\nu_5(T_{2g})$ [$A_g + 2B_g + A_u + 2B_u$]. Likewise, the infrared-active bands of the triply degenerate $\nu_3(T_{1u})$, $\nu_4(T_{1u})$, and $\nu_6(T_{2u})$ modes under O_h symmetry are each predicted to be split into Raman-active g-components and infrared-active u-components [$A_g + 2B_g + A_u + 2B_u$]. Accordingly, in the Raman spectra (Figure 3 and Table 3), $\nu_1(A_{1g})$ is unsplit [A_g], $\nu_2(E_g)$ is split into two components [$2A_g$], $\nu_3(T_{1u})$ is rendered Raman-active and is split into three components [$A_g + 2B_g$], with the most intense band assigned to the A_g component. Only two of the expected three components [$A_g + 2B_g$] are resolved for $\nu_5(T_{2g})$, where the more intense band is assigned to the A_g component and is presumed to overlap with one of the B_g components. The $A_g + 2B_g$ components of $\nu_4(T_{1u})$ (out of SbF_4-plane umbrella bends under O_h symmetry) are apparently too

Scheme 1. Representative Thermochemical Cycles Describing the Reactions of BrO_3F with SbF_5 That Lead to $[BrO_3][SbF_6]$ and $[BrO_2][SbF_6]$

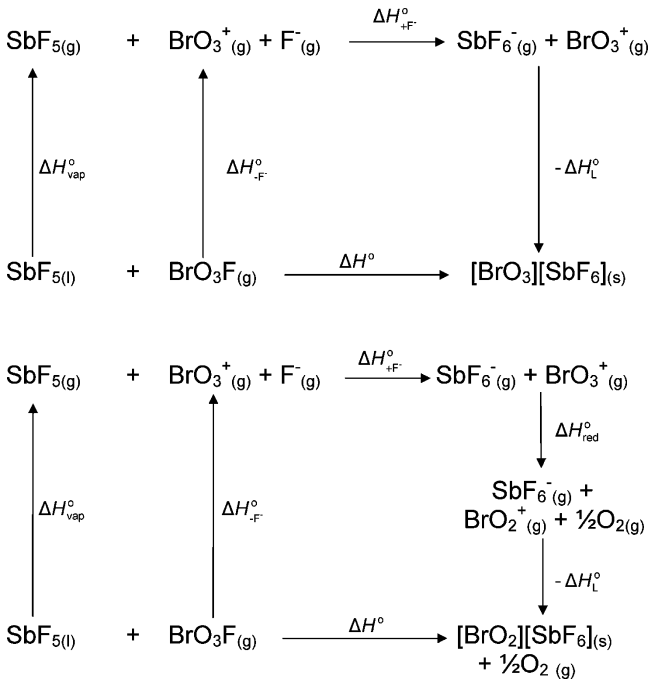

weak to be observed and/or may overlap with the $\nu_5(T_{2g})$ components (in SbF_4-plane scissors bends under O_h symmetry), which are expected to have similar frequencies. The assignment for $\nu_6(T_{2u})$ is tentative, with the single observed band attributed to the A_g factor-group component.

Several bands of moderate intensity were observed below 210 cm^{-1} in the Raman spectra of $[XO_2][SbF_6]$ (X = Cl, Br) which have been assigned to modes associated with the four secondary bonding interactions that occur between each cation and four anions in the crystal lattices of these salts (see footnote c of Table 3, Results and Discussion, and Supporting Information, Tables S4 and S5).

Computational Results

(a) Thermodynamic Evaluation of Reactions Between XO_3F and XO_2F (X = Cl, Br) and the Lewis Acids SbF_5 and AsF_5. It has previously been noted that the reactivities and amphoteric behaviors of chlorine oxide fluorides are predominantly determined by their structures and those of the cation or anion that is formed rather than by the relative fluoride ion donor−acceptor strengths of the parent chlorine oxide fluorides.[40] Accordingly, the tetrahedral structure of ClO_3F is favored over either a trigonal planar ClO_3^+ cation or a trigonal bipyramidal $ClO_3F_2^-$ anion. The validity of this generalization is supported by the present experimental work and the thermochemical calculations presented in this section.

Attempts to prepare $[BrO_3][Sb_nF_{5n+1}]$ by the reaction of liquid SbF_5 with BrO_3F were unsuccessful, resulting in the reduction of Br(VII) and the isolation of BrO_2^+ salts. This contrasts with ClO_3F, which fails to react with liquid SbF_5 at ambient temperature. To account for the different reactivities of ClO_3F and BrO_3F, quantum-chemical calculations and established semiempirical methods[59–63] were used in conjunction with known thermodynamic quantities to estimate $\Delta H°$, $\Delta S°$, and $\Delta G°$ for eqs 5 and 6.

$$XO_3F + (MF_5)_n \rightarrow [XO_3][M_nF_{5n+1}] \qquad (M = As, Sb) \tag{5}$$

$$XO_3F + (MF_5)_n \rightarrow [XO_2][M_nF_{5n+1}] + {}^1/_2O_2 \qquad (M = As, Sb) \tag{6}$$

The standard enthalpies for these reactions were determined by analyzing their Born−Haber cycles (Scheme 1). The enthalpy changes for the gas-phase fluoride ion transfer reactions among the halogen oxide fluorides and Lewis acids were calculated by use of eq 7,

$$\Delta H°_{F^-} = \Delta H°_{-F^-} + \Delta H°_{+F^-} \tag{7}$$

where the enthalpies of fluoride ion abstraction ($\Delta H°_{-F^-}$) from the perhalyl fluorides and the enthalpies of fluoride ion attachment ($\Delta H°_{+F^-}$) to the Lewis acids were calculated by several methods up to and including the CCSD(T) method (Table 4). The gas-phase enthalpies of reduction for the XO_3^+ cations corresponding to eq 8 were also calculated at the same level (Table 4).

$$XO_3^+ \rightarrow XO_2^+ + {}^1/_2O_2 \tag{8}$$

The enthalpy of vaporization ($\Delta H°_{vap}$) is zero for AsF_5 because it is a gas under standard conditions but must be accounted for in reactions involving SbF_5, which is a viscous liquid at ambient temperature. The determination of $\Delta H°_{vap}$ for $n SbF_{5(l)}$ ($n = 1-3$) is complicated by the polymeric nature of liquid SbF_5 and the predominance of the $(SbF_5)_3$ trimer in the gas phase at ambient temperature.[67] Using the enthalpy of vaporization for $(SbF_5)_3$ (43.4 kJ mol^{-1})[68] and the dissociation energy reported for ${}^1/_4(SbF_5)_4$ to SbF_5 (18.5 kJ mol^{-1}),[69] the enthalpy of vaporization for monomeric SbF_5 has previously been estimated to be 30.9 kJ mol^{-1}.[70] A

(59) Bartlett, N.; Yeh, S.; Kourtakis, K.; Mallouk, T. *J. Fluorine Chem.* **1984**, *26*, 97–116.
(60) Shen, C.; Hagiwara, R., Mallouk, T. E.; Bartlett, N. In *Inorganic Fluorine Chemistry, Toward the 21st Century*; Thrasher, J. S., Strauss, S. H. , Eds.; ACS Symposium Series 555; Washington, DC, 1994; Chapter 2, pp 26−39.
(61) Jenkins, H. D. B.; Tudela, D.; Glasser, L. *Inorg. Chem.* **2002**, *41*, 2364–2367.
(62) Jenkins, H. D. B.; Roobottom, H. K.; Passmore, J.; Glasser, L. *Inorg. Chem.* **1999**, *38*, 3609–3620.
(63) Jenkins, H. D. B.; Glasser, L. *Inorg. Chem.* **2003**, *42*, 8702–8708.
(64) Christe, K. O.; Dixon, D. A.; McLemore, D.; Wilson, W. W.; Sheehy, J. A.; Boatz, J. A. *J. Fluorine Chem.* **2000**, *101*, 151–153.
(65) Christe, K. O. ; Dixon, D. A. 16th Winter Fluorine Conference, St. Petersburg, FL, Jan. 12−17, **2003**.
(66) Krossing, I.; Raabe, I. *Chem.—Eur. J.* **2004**, *10*, 5017–5030.
(67) Brunvoll, J.; Ishchenko, A. A.; Myakshin, I. N.; Romanov, G. V.; Spiridonov, V. P.; Strand, T. G.; Sukhoverkhov, V. F. *Acta Chem. Scand., A* **1980**, *34*, 733–737.
(68) Shair, R. C.; Schurig, W. F. *J. Ind. Eng. Chem.* **1951**, *43*, 1624–1627.
(69) Fawcett, J.; Holloway, J. H.; Peacock, R. D.; Russell, D. K. *J. Fluorine Chem.* **1982**, *20*, 9–12.
(70) Bougon, R.; Bui Huy, T.; Burgess, J.; Christe, K. O.; Peacock, R. D. *J. Fluorine Chem.* **1982**, *19*, 263–277.

Table 4. Enthalpies of Reaction Determined for Gas-Phase Fluoride Ion Transfer Reactions Involving BrO_3F, ClO_3F, BrO_2F, ClO_2F, AsF_5, and Sb_nF_{5n} ($n = 1-3$)

		G2[a]	B3LYP[b]	CCSD(T)[c]	MP2[d]	CCSD[d]	CCSD(T)[d]	lit
F^- detachment				$\Delta H^\circ_{-F^-}$ (kJ mol^{-1})				
	$BrO_3F_{(g)} \rightarrow BrO_3^+{}_{(g)} + F^-_{(g)}$	1005	993 (989)	997	968	1037	1006	
	$ClO_3F_{(g)} \rightarrow ClO_3^+{}_{(g)} + F^-_{(g)}$	999	974 (966)	981	970	1014	995	
	$BrO_2F_{(g)} \rightarrow BrO_2^+{}_{(g)} + F^-_{(g)}$	903	910 (908)	890	856	919	899	
	$ClO_2F_{(g)} \rightarrow ClO_2^+{}_{(g)} + F^-_{(g)}$	895	889 (886)	872	858	890	883	
F^- attachment				$\Delta H^\circ_{+F^-}$ (kJ mol^{-1})				
	$AsF_{5(g)} + F^-_{(g)} \rightarrow AsF_6^-{}_{(g)}$	−439	−402 (−404)	−436	−427	−438	−435	−443[e] −426[g]
	$SbF_{5(g)} + F^-_{(g)} \rightarrow SbF_6^-{}_{(g)}$		−461 (−465)	−504	−496	−510	−505	−503[e] −489[g]
	$Sb_2F_{10(g)} + F^-_{(g)} \rightarrow Sb_2F_{11}^-{}_{(g)}$		−516 (−521)					−531[f] −549[g]
	$Sb_3F_{15(g)} + F^-_{(g)} \rightarrow Sb_3F_{16}^-{}_{(g)}$		−541 (−544)					−551[f] −582[g]
halogen reduction				ΔH°_{red} (kJ mol^{-1})				
	$BrO_3^+{}_{(g)} \rightarrow BrO_2^+{}_{(g)} + ½O_{2(g)}$	−215	−239 (−240)	−232	−247	−242	−225	
	$ClO_3^+{}_{(g)} \rightarrow ClO_2^+{}_{(g)} + ½O_{2(g)}$	−145	−171 (−185)	−178	−159	−163	−155	

[a] Calculated using the G2 method implemented in Gaussian 98, no basis-set is available in this method for Sb. [b] ZPE-corrected enthalpies at B3LYP/aug-cc-pVQZ level, values in parentheses are with aug-cc-pVTZ. [c] CCSD(T)/aug-cc-pVTZ. [d] Single-point aug-cc-pVQZ calculation using the B3LYP/aug-cc-pVTZ optimized structure. [e] MP2/PDZ in ref 64 [f] MP2/PDZ in ref 65 [g] MP2/TZVPP in ref 66.

similar approach estimates the enthalpy of vaporization to be 38.1 kJ mol^{-1} for Sb_2F_{10}. The lattice enthalpies of the proposed XO_3^+ and XO_2^+ salts (Table 5) were estimated by use of the volume-based method of Bartlett et al.[21,59,60] as generalized by Jenkins et al.[61,62] in eq 9,

$$H^\circ_L = 2I\left(\frac{\alpha}{\sqrt[3]{V_m}} + \beta\right) + pRT \qquad (9)$$

where R is the gas constant (8.314 J K^{-1} mol^{-1}), I is the ionicity of the salt, and the constants α, β, and n depend on the nature of the salt. For the salts under investigation, which are singly charged and nonlinear, the following values have been used: $I = 1$, $\alpha = 117.3$ mm kJ mol^{-1}, $\beta = 51.9$ kJ mol^{-1}, and $p = 2$. In this formalism, H°_L is the lattice enthalpy and is defined as the energy required to break the crystal lattice and therefore has a positive value. This approach is generally accurate to ~4% for salts with H°_L less than 5000 kJ mol^{-1} [62] and is particularly useful because the unit molar volume (V_m) of an unknown salt can be estimated with reasonable accuracy using several methods.[62,72] The net enthalpies of reaction (eq 10)

$$\Delta H^\circ = \Delta H^\circ_{vap} + \Delta H^\circ_{F^-} + \Delta H^\circ_{red} - H^\circ_L \qquad (10)$$

calculated for the formations of the XO_3^+ and XO_2^+ salts by the reaction of the perhalyl fluorides with $AsF_{5(g)}$ and $nSbF_{5(l)}$ ($n = 1-3$) are summarized in Table 6.

Table 5. Estimated Lattice Enthalpies of Salts Containing the XO_3^+ and XO_2^+ (X = Cl, Br) Cations

salt	V_m (nm^3)[a]	ΔH°_L (kJ mol^{-1})[b]	S° (J mol^{-1} K^{-1})[c]
$[BrO_3][AsF_6]$	0.151	545	220
$[BrO_3][SbF_6]$	0.162	539	235
$[BrO_3][Sb_2F_{11}]$	0.268	473	379
$[BrO_3][Sb_3F_{16}]$	0.374	434	524
$[ClO_3][AsF_6]$	0.147	553	215
$[ClO_3][SbF_6]$	0.158	543	230
$[ClO_3][Sb_2F_{11}]$	0.264	475	374
$[ClO_3][Sb_3F_{16}]$	0.370	436	518
$[BrO_2][AsF_6]$	0.142	558	208
$[BrO_2][SbF_6]$	0.153	547	223
$[BrO_2][Sb_2F_{11}]$	0.259	477	367
$[BrO_2][Sb_3F_{16}]$	0.365	437	511
$[ClO_2][AsF_6](s)$	0.138	563	203
$[ClO_2][SbF_6](s)$	0.149	551	218
$[ClO_2][Sb_2F_{11}](s)$	0.255	479	362
$[ClO_2][Sb_3F_{16}](s)$	0.361	438	506

[a] The formula unit volumes, V_m, for $[ClO_2][SbF_6]$ (0.149 nm^3) and $[BrO_2][SbF_6]$ (0.153 nm^3) were obtained from their crystallographic unit cells at −173 °C. The volumes of ClO_2^+ (0.028 nm^3) and BrO_2^+ (0.032 nm^3) were estimated by substitution of the volume of the SbF_6^- anion (0.121 nm^3, ref 62), from V_m. The estimated volume of ClO_3^+ (0.037 nm^3) was obtained from ref 72. The average difference in volumes of NO_n^+ ($n = 1$, 2) and ClO_n^+ ($n = 2$, 3) is 0.009 nm^3 and was used to estimate the volume of BrO_3^+ (0.041 nm^3) from the volume of BrO_2^+. The values of V_m for the remaining XO_2^+ and XO_3^+ salts were estimated from the sums of the cation and anion volumes (AsF_6^-, 0.110 nm^3, ref 62; $Sb_2F_{11}^-$, 0.227 nm^3, ref 71; $Sb_3F_{16}^-$, 0.333 nm^3, ref 71). [b] The lattice enthalpies (ΔH°_L) were calculated as described in ref 61. [c] The standard entropies were calculated as described in ref 63.

A method for estimating the absolute standard entropy of a salt from its unit volume has been reported by Jenkins and

(71) Elliott, H. S.; Lehmann, J. F. ; Mercier; H. P. A. Jenkins, H. D. B.; Schrobilgen, G. J. Unpublished results.

(72) Jenkins, H. D. B.; Glasser, L.; Klapötke, T. M.; Crawford, M.-J.; Bhasin, K. K.; Lee, J.; Schrobilgen, G. J.; Sunderlin, L. S.; Liebman, J. F. *Inorg. Chem.* **2004**, *43*, 6238–6248.

Table 6. Values of $\Delta H°$, $\Delta S°$, and $\Delta G°$ Calculated for Reactions Leading to Selected XO_3^+ and XO_2^+ Salts (X = Cl, Br) with AsF_5 and $nSbF_5$ (n = 1−3)

	$\Delta H°$ (kJ mol^{-1})		$\Delta S°$ (J mol^{-1} K^{-1})	$\Delta G°$ (kJ mol^{-1})	
Formation of XO_3^+ Salts from XO_3F:					
$BrO_3F_{(g)} + AsF_{5(g)} \rightarrow [BrO_3][AsF_6]_{(s)}$	16[a]	26[c]	−566	185[a]	195[c]
$BrO_3F_{(g)} + SbF_{5(l)} \rightarrow [BrO_3][SbF_6]_{(s)}$	−6[b]	−7[c]	−329	92[b]	91[c]
$BrO_3F_{(g)} + 2SbF_{5(l)} \rightarrow [BrO_3][Sb_2F_{11}]_{(s)}$	39[b]	52[d]	−450	173[b]	186[d]
$BrO_3F_{(g)} + 3SbF_{5(l)} \rightarrow [BrO_3][Sb_3F_{16}]_{(s)}$	63[b]	75[d]	−570	233[b]	244[d]
$ClO_3F_{(g)} + AsF_{5(g)} \rightarrow [ClO_3][AsF_6]_{(s)}$	6[a]	7[c]	−551	170[a]	171[c]
$ClO_3F_{(g)} + SbF_{5(l)} \rightarrow [ClO_3][SbF_6]_{(s)}$	−16[b]	−22[c]	−314	78[b]	71[c]
$ClO_3F_{(g)} + 2SbF_{5(l)} \rightarrow [ClO_3][Sb_2F_{11}]_{(s)}$	31[b]	39[d]	−435	161[b]	168[d]
$ClO_3F_{(g)} + 3SbF_{5(l)} \rightarrow [ClO_3][Sb_3F_{16}]_{(s)}$	55[b]	62[d]	−556	221[b]	227[d]
Formation of XO_2^+ Salts from XO_3F:					
$BrO_3F_{(g)} + AsF_{5(g)} \rightarrow [BrO_2][AsF_6]_{(s)} + 1/2O_{2(g)}$	−208[a]	−212[a]	−475	−66[a]	−70[c]
$BrO_3F_{(g)} + SbF_{5(l)} \rightarrow [BrO_2][SbF_6]_{(s)} + 1/2O_{2(g)}$	−229[b]	−240[c]	−238	−158[b]	−169[c]
$BrO_3F_{(g)} + 2SbF_{5(l)} \rightarrow [BrO_2][Sb_2F_{11}]_{(s)} + 1/2O_{2(g)}$	−183[b]	−177[d]	−359	−76[b]	−70[d]
$BrO_3F_{(g)} + 3SbF_{5(l)} \rightarrow [BrO_2][Sb_3F_{16}]_{(s)} + 1/2O_{2(g)}$	−155[b]	−153[d]	−480	−12[b]	−10[d]
$ClO_3F_{(g)} + AsF_{5(g)} \rightarrow [ClO_2][AsF_6]_{(s)} + 1/2O_{2(g)}$	−149[a]	−158[a]	−460	−12[a]	−21[c]
$ClO_3F_{(g)} + SbF_{5(l)} \rightarrow [ClO_2][SbF_6]_{(s)} + 1/2O_{2(g)}$	−170[b]	−185[c]	−223	−104[b]	−119[d]
$ClO_3F_{(g)} + 2SbF_{5(l)} \rightarrow [ClO_2][Sb_2F_{11}]_{(s)} + 1/2O_{2(g)}$	−117[b]	−120[d]	−344	−1[b]	−18[d]
$ClO_3F_{(g)} + 3SbF_{5(l)} \rightarrow [ClO_2][Sb_3F_{16}]_{(s)} + 1/2O_{2(g)}$	−92[b]	−95[d]	−465	47[b]	43[d]
Formation of $[XO_2][SbF_6]$ from XO_2F:					
$BrO_2F_{(g)} + SbF_{5(l)} \rightarrow [BrO_2][SbF_6]_{(s)}$	−116[b]	−122[c]	−336	−16[b]	−22[c]
$ClO_2F_{(g)} + SbF_{5(l)} \rightarrow [ClO_2][SbF_6]_{(s)}$	−128[b]	−143[c]	−326	−31[b]	−46[c]

[a] Values computed by use of G2 theory. [b] Because the G2 method implemented in Gaussian 98 had no basis set available for Sb, gas-phase G2 enthalpies of fluoride ion attachment ($\Delta H°_{+F^-}$) are therefore unavailable for Sb_nF_{5n} and $Sb_nF_{5n+1}^-$. Instead, values from refs 64 and 65 have been used. [c] Values computed by use of CCSD(T) method. [d] Because of the sizes of $Sb_2F_{11}^-$ and $Sb_3F_{16}^-$, no CCSD(T) calculation was possible, instead, the DFT functional, B3LYP, was used.

Glasser (eq 11).[63] Entropies of the XO_2^+ and XO_3^+ salts under consideration

$$S°([XO_3][MF_6]) = kV_m + c \quad (11)$$

are provided in Table 5. When coupled with the experimental standard entropies of $BrO_3F_{(g)}$ (299 J mol^{-1} K^{-1}),[73] $BrO_2F_{(g)}$ (294 J mol^{-1} K^{-1}),[74] $ClO_3F_{(g)}$ (279 J mol^{-1} K^{-1}),[75] $ClO_2F_{(g)}$ (279 J mol^{-1} K^{-1}),[74] $AsF_{5(g)}$ (487 J mol^{-1} K^{-1}),[76] $SbF_{5(l)}$ (265 J mol^{-1} K^{-1}),[76] and $O_{2(g)}$ (206 J mol^{-1} K^{-1}),[75] this method allows $\Delta S°$ (eqs 12, 13) and $\Delta G°$ (eq 14) to be calculated for the reactions of interest. The $\Delta S°$ and $\Delta G°$

$$\Delta S° = S°([XO_3][MF_6]) - S°(MF_5) - S°(XO_3F) \quad (12)$$

$$\Delta S° = S°([XO_2][MF_6]) + {}^1/_2 S°(O_2) - nS°(MF_5) - S°(XO_3F) \quad (13)$$

$$\Delta G° = \Delta H° - T\Delta S° \quad (14)$$

values obtained for these reactions are summarized in Table 6. Based on these calculations, the large enthalpies of fluoride ion abstraction from BrO_3F and ClO_3F are nearly counter balanced by the enthalpies of fluoride ion attachment to the Lewis acids and the lattice energies of the products, resulting in net reaction enthalpies that approach thermal neutrality ($\Delta H°$ −22 to 75 kJ mol^{-1}) but are generally weakly endothermic (Table 6).

The entropy term, which is often assumed to have a small effect on $\Delta G°$, increases the endothermicities of these reactions by 98 to 170 kJ mol^{-1}. Consequently, the inability to prepare BrO_3^+ and ClO_3^+ salts by the reaction of the perhalyl fluoride with strong fluoride ion acceptors is consistent with the positive $\Delta G°$ values calculated for the reactions of BrO_3F (92−244 kJ mol^{-1}) and ClO_3F (71−227 kJ mol^{-1}) with AsF_5(g) and $nSbF_5$(l) (n = 1−3). Interestingly, there are distinct minima in $\Delta H°$, $\Delta S°$, and $\Delta G°$ for the reactions that lead to $[XO_3][SbF_6]$ salts, indicating that the benefits of using Lewis acids having higher fluoride ion affinities, as in the case of Sb_2F_{10} and Sb_3F_{16}, are offset by the lower lattice energies and greater entropies of the resulting $Sb_2F_{11}^-$ and $Sb_3F_{16}^-$ salts.

With the exception of the reaction of ClO_3F with Sb_3F_{15} leading to $[ClO_2][Sb_3F_{16}]$, which is predicted to be mildly endothermic ($\Delta G°$, 43 kJ mol^{-1}), all other reactions involving the reduction of the perhalyl fluorides and the formation of the BrO_2^+ (−10 to −169 kJ mol^{-1}) and ClO_2^+ (−1 to −119 kJ mol^{-1}) salts are predicted to be exothermic (Table 6). The differences between the $\Delta G°$ values corresponding to the formation of the XO_3^+ and XO_2^+ salts are primarily the result of the large gas-phase enthalpies of reduction for BrO_3^+ (−215 and −255 kJ mol^{-1} at the G2 and CCSD(T) level, respectively) and ClO_3^+ (−145 and −155 kJ mol^{-1} at G2 and CCSD(T) level, respectively) (Table 4). The higher lattice energies for the XO_2^+ salts and smaller entropy changes associated with the formation of these salts also make significant contributions. The greater magnitude of $\Delta H°_{red}$ for BrO_3^+ compared with that of ClO_3^+ is in agreement with the observation that ClO_3F fails to react with $SbF_{5(l)}$, whereas the reaction of BrO_3F with $SbF_{5(l)}$ is spontaneous and rapid. The failure of BrO_3F to undergo reductive elimination of O_2 in a HF solution of SbF_5 or in neat AsF_5, along with the general inertness of ClO_3F, suggests that a kinetic barrier may impede reaction in these media and that the barrier is only overcome or reduced in the presence of $(SbF_5)_n$ (n > 1), producing $[BrO_2][Sb_nF_{5n+1}]$, which can be subsequently converted to the more stable $[BrO_2][SbF_6]$ salt. The inertness of ClO_3F may be attributed

(73) Johnson, G. K.; O'Hare, P. A. G.; Appelman, E. H. *Inorg. Chem.* **1972**, *11*, 800–802.
(74) Christe, K. O.; Curtis, E. C.; Jacob, E. *Inorg. Chem.* **1978**, *17*, 2744–2749.
(75) Chase, M. W., Jr. *NIST JANAF Thermochemical Tables*; American Institute of Physics: New York, 1998.
(76) (a) O'Hare, P. A. G. *J. Chem. Thermodyn.* **1993**, *25*, 391–402. (b) Nagarajan, G. *Bull. Soc. Chim. Belg.* **1962**, *71*, 324–328.

Table 7. Calculated Bond Lengths (Å) and Bond Angles (°) for the XO_3^+ and XO_2^+ (X = Cl, Br) Cations

	XO_2^+				XO_3^+			
method	Br−O	O−Br−O	Cl−O	O−Cl−O	Br−O	O−Br−O	Cl−O	O−Cl−O
exptl.[a]	1.595(2)	112.0(1)	1.381(7)	117.7(5)				
exptl.[b]	1.6135	117.5	1.410(2)	118(9)				
HF/6−311G(d)	1.529	116.1	1.372	119.9	1.537	120.0	1.372	120.0
MP2/6−311G(d)	1.635	118.6	1.478	121.8	1.601	120.0	1.478	120.0
QCISD/6−311G(2d)	1.603[c]	116.1[c]	1.426	121.0	1.595	120.0	1.416	120.0
CCSD(T)/aug-cc-pVTZ	1.614	115.4	1.443	120.2	1.603	120.0	1.430	120.0
MPW1PW91/DZVP	1.607	116.3	1.435	120.4	1.609	120.0	1.434	120.0
B3LYP/aug-cc-pVTZ	1.595	115.7	1.428	120.3	1.599	120.0	1.427	120.0
B3LYP/aug-cc-pVQZ	1.591	115.6	1.417	120.9	1.595	120.0	1.415	120.0

[a] Experimental values for $[XO_2][SbF_6]$ are taken from Table 2 [b] Experimental values for gaseous BrO_2^+ and ClO_2^+ in solid Cl_2O_6 are from refs 45 and 18, respectively. [c] ref 45.

to the near-zero free energy change calculated for the formation of $[ClO_2][Sb_2F_{11}]$ (Table 6) and to the likelihood that the kinetic barrier is higher for ClO_3F than for BrO_3F. The latter hypothesis is consistent with the general inertness of ClO_3F illustrated by its failure to react with metallic sodium at temperatures as high as 300 °C[77] and strong fluoride ion donors such as $[N(CH_3)_4][F]$,[34] NO_2F,[40] and CsF.[40]

In view of the high enthalpies of fluoride ion abstraction calculated for XO_3F, which contributed to the inability to prepare XO_3^+ salts, the stabilities of the $[XO_2][SbF_6]$ salts with respect to dissociation (eq 15) were also considered. The thermochemistries of these reactions (Table 6)

$$[XO_2][MF_6] \rightarrow XO_2F + SbF_5 \qquad (15)$$

were investigated by analogy with the method used to investigate the formation of the $[XO_3][SbF_6]$ salts using the known standard entropies of BrO_2F (294 J mol^{-1} K^{-1})[74] and ClO_2F (279 J mol^{-1} K^{-1}).[74] The calculated free energies of reaction for $[BrO_2][SbF_6]$ (−22 kJ mol^{-1} at CCSD(T) level) and $[ClO_2][SbF_6]$ (−46 kJ mol^{-1} at CCSD(T) level) from XO_2F and SbF_5 are somewhat negative indicating that both salts are stable under standard conditions (Table 6). The stabilities of $[BrO_2][SbF_6]$ and $[ClO_2][SbF_6]$ are in qualitative agreement with the stabilities of $[BrO_2][SbF_6]$, $[BrO_2][Sb_{22.4}F_{12.2}]$,[24] $[ClO_2][SbF_6]$,[78] $[ClO_2][Sb_2F_{11}]$,[19] $[ClO_2][RuF_6]$,[22] and $[ClO_2][AsF_6]$[17] at ambient temperature and the instabilities noted for $[BrO_2][AsF_6]$,[25,26] $[BrO_2][BF_4]$,[25] and $[ClO_2][BF_4]$.[17,20] The XO_2^+ salts contrast with the unknown XO_3^+ salts in this respect, because the latter salts are enthalpically unstable with respect to dissociation to XO_3F and the parent Lewis acid and therefore are not stabilized by reduction of the $T\Delta S°$ term.

(b) Geometries of XO_2^+ and XO_3^+. The energy-minimized geometries of the XO_2^+ and XO_3^+ cations, calculated by use of the HF, MP2, MPW1PW91, B3LYP, QCISD, and CCSD(T) methods, are listed in Table 7. A comparison of the calculated geometries of BrO_2^+ and ClO_2^+ with those obtained from the crystal structures of their SbF_6 salts (Table 2) reveals similar trends for both cations despite secondary bonding interactions with four neighboring anions in the crystal lattice (see Crystal Structures). The experimental X−O bond lengths of the XO_2^+ cations are bracketed by the HF and MP4 methods, which under- and overestimate the bond lengths, respectively. Møller−Plesset perturbation theory (MP2 and MP4) generally overestimates the experimental bond lengths of BrO_2^+ and ClO_2^+ (Tables 7 and S6).[47] The CCSD(T) calculation is in agreement with the experimental Br−O bond length of BrO_2^+ (Table 7) and also supports previous quantum-chemical studies at the QCISD[47] and CCSD(T)[45,47] levels. Density functional theory calculations, especially the B3LYP functional in combination with the aug-cc-pVTZ basis set, are in excellent agreement with the experimental bond distance of BrO_2^+ (Tables 7 and Supporting Information, Table S6). Interestingly, the relatively short Cl−O bond lengths obtained in the crystal structure of $[ClO_2][SbF_6]$ of 1.28(3) Å is overestimated for all quantum-chemical levels used in this study. The best estimate of the Cl−O bond distance, calculated at the HF level, is 0.1 Å longer than the experimental value. The calculated values are in overall better agreement with the experimental Cl−O bond distance of 1.410(2) Å in $[ClO_2][ClO_4]$.[18] This contrasts with the excellent agreement obtained for the BrO_2^+ cation when the same methods are employed.

The bond angles of the XO_2^+ cations were overestimated by 2 to 5° by each of the computational methods used in the present and previous studies; however, the small ranges among the calculated O−Br−O (116.1−118.6°) and O−Cl−O (119.9−121.8°) angles suggest that this parameter is essentially insensitive to the computational method (Table 7).

The inability to prepare and structurally characterize XO_3^+ salts prevents comparisons with experimental bond lengths. On the basis of the trends noted for the XO_2^+ cations (vide supra), the X−O bond lengths are predicted to lie within the ranges defined by 1.537 (HF) −1.609 (MPW1PW91) Å for BrO_3^+ and 1.372 (HF) −1.478 (MP2) Å for ClO_3^+ and are likely very similar to the values obtained using the CCSD(T) [1.603 (Br), 1.430 (Cl) Å] and B3LYP [1.599 (Br), 1.415 Cl) Å] levels (Table 7).

The bond lengths predicted for the XO_3^+ cations are consistently shorter than those of the $BrO_3F_2^-$ (HF, 1.590; MPW1PW91, 1.639 Å) and $ClO_3F_2^-$ (HF, 1.431; MPW1PW91, 1.465 Å) determined by the same method.[34] The shorter bond lengths predicted for the XO_3^+ cations, which also have

(77) Engelbrecht, A.; Atzwanger, H. *J. Inorg. Nucl. Chem.* **1956**, *2*, 348–357.
(78) This work.

Table 8. Calculated Vibrational Frequencies[a] for the BrO_3^+ and ClO_3^+ Cations

assgnt	description[b]	HF[c,d]	sca. HF[e]	MP2[c,d]	QCISD	CCSD(T)	MPW1PW91[d,e]	B3LYP[d]
				BrO_3^+				
$\nu_1(A_1')$	$\nu_s(BrO_3)$	964.6(44)[0]	863.7	908.0(50)[0]	824.8[0]	821.3	855.4(39)[0]	849.6(44)[0]
$\nu_2(A_2'')$	$\delta(BrO_3)$ o.o.p	292.7(0)[24]	262.1	272.8(0)[6]	241.0[7]	223.4	251.2(0)[8]	230.6(0)[9]
$\nu_3(E')$	$\nu_{as}(BrO_3)$	1054.1(4)[94]	943.8	1251.4(72)[14]	920.3[22]	955.3	974.9(10)[46]	966.3(8)[15]
$\nu_4(E')$	$\delta(BrO_2)$ i.p	390.3(4)[56]	349.5	334.3(6)[24]	331.6[26]	323.2	319.3(5)[24]	328.6(14)[11]
				ClO_3^+				
$\nu_1(A_1')$	$\nu_s(ClO_3)$	1125.1(40)[0]	1007.4	910.0(32)[0]	949.5[0]	924.9	964.3(37)[0]	973.1(38)[0]
$\nu_2(A_2'')$	$\delta(ClO_3)$ o.o.p.	508.8(0)[40]	455.6	427.5(0)[10]	467.8[12]	431.7	433.3(0)[14]	451.9(0)[12]
$\nu_3(E')$	$\nu_{as}(ClO_3)$	1441.9(5)[372]	1291.1	1390.0(58)[28]	1258[136]	1250.5	1278.0(9)[160]	1290.5(7)[66]
$\nu_4(E')$	$\delta(ClO_2)$ i.p.	580.2(4)[78]	519.5	462.1(8)[42]	510.4[20]	487.7	484.0(5)[42]	508.6(17)[17]

[a] Frequencies in cm^{-1} and calculated at the levels HF/6−311G(d), MP2/6−311G(d), QCISD/6−311G(2d), CCSD(T)/aug-cc-pVTZ, MPW1PW91/DZVP, and B3LYP/aug-cc-pVQZ. [b] Symbols denote symmetric stretch (ν_s), asymmetric stretch (ν_{as}), and bend (δ). Abbreviations denote out-of-plane (o.o.p.) and in-plane (i.p.) [c] Calculated Raman intensities ($Å^4$ amu^{-1}) are given in parentheses. [d] Calculated infrared intensities (km mol^{-1}) are in square brackets. [e] Scaled by 0.8953 as recommended in ref 58.

trigonal planar oxygen arrangements, are attributed to their net positive charges that result in shorter and less polar X−O bonds.

(c) Vibrational Frequencies of XO_2^+ and XO_3^+. (i) ClO_2^+ and BrO_2^+. Two prior studies have investigated the vibrational frequencies of the BrO_2^+ cation using the MP2, MP4, QCISD, and CCSD(T) methods with various basis sets[45,47] (Supporting Information, Table S7). These studies did not include the computationally less demanding HF and density functional methods. Although several ClO_2^+ salts have been structurally characterized, the vibrational frequencies of this cation have not been calculated. In the present study, the vibrational frequencies of the BrO_2^+ and ClO_2^+ cations have been calculated by the HF, MPW1PW91, B3LYP, MP2, QCISD, and CCSD(T) methods (Table 3). The HF frequencies are not considered in the ensuing discussion.

The vibrational frequencies obtained for the XO_2^+ cations using the MPW1PW91 and B3LYP methods are in reasonable agreement with the experimental frequency ranges. Using these methods, the $\nu_1(A_1)$ and $\nu_3(B_2)$ stretching frequencies of BrO_2^+ were overestimated by ∼63 and ∼73 cm^{-1}, respectively, while the $\nu_2(A_1)$ bending mode was underestimated by 21 cm^{-1} using MPW1PW91 and by 10 cm^{-1} using the B3LYP functional. The same trends were obtained for ClO_2^+ using these methods (Table 3).

The frequencies corresponding to the $\nu_1(A_1)$ and $\nu_2(A_1)$ modes of BrO_2^+ do not exhibit strong basis set dependencies and were calculated with reasonable accuracy, whereas the frequency of $\nu_3(B_2)$ decreased substantially as the quality of the basis set improved and only came within 45 cm^{-1} of the experimental range when the TZVP basis set was used. The vibrational frequencies of the BrO_2^+ cation obtained by the MP4/TZVP method are less accurate than those obtained by the MP2/TZVP method[47] (Supporting Information, Table S7). The vibrational frequencies of the ClO_2^+ cation exhibit little variation for the two basis sets that were investigated (6−31G*, 6−311G(d)) using the MP2 method.

The present quantum-chemical calculations of the vibrational frequencies at the CCSD(T) level are in good agreement with experimental frequencies and previous results which used the QCISD and CCSD(T) levels for the vibrational frequencies of BrO_2^+.[45,47] Both methods exhibited minor basis set dependencies resulting in positive frequency shifts for each of the three vibrational modes of BrO_2^+ as the quality of the basis set improved. The best correlation for the BrO_2^+ cation was obtained from the QCISD/6−31G(2d) method, which provided $\nu_1(A_1)$ and $\nu_3(B_2)$ stretching frequencies within the experimental range and underestimated the $\nu_2(A_1)$ frequency by 22 cm^{-1}. The calculated frequency shifts for[79,81] BrO_2^+ isotopomers are in excellent agreement with the experimental spectrum of $[BrO_2][SbF_6]$, in which cation band splitting is only observed for the asymmetric stretch (Table 3). The use of the QCISD method in combination with the 6−311G(2d) basis set for ClO_2^+ again provides the best correlation with experimental spectra (Table 3), with $\nu_1(A_1)$ and $\nu_2(A_1)$ being underestimated by 19 and 14 cm^{-1}, respectively, and $\nu_3(B_2)$ lying within the observed range. The calculated isotopic splittings for the $\nu_1(A_1)$ and $\nu_3(B_2)$ stretching modes are in good agreement with those observed experimentally; however, the 4 cm^{-1} splitting calculated for $\nu_2(A_2)$ could not be resolved in the Raman spectra of the ClO_2^+ salts (Figure 3b).

(ii) ClO_3^+ and BrO_3^+. The trigonal planar XO_3^+ cations have six fundamental modes of vibration ($\Gamma_{vib} = A_1' + A_2'' + 2E'$) corresponding to three Raman-active bands (A_1', $2E'$) and three infrared-active bands (A_2'', $2E'$). The vibrational frequencies of the XO_3^+ cations have been calculated by the HF, MPW1PW91, B3LYP, MP2, QCISD, and CCSD(T) methods (Table 8). The QCISD/6−311G(2d) frequencies are expected to be the most reliable based on the XO_2^+ cation results (vide supra). The $\nu_1(A_1)$ and $\nu_3(B_2)$ XO_2 stretching frequencies obtained using the MPW1PW91 and B3LYP methods are moderately higher than those obtained by the QCISD method, suggesting that correlations between the experimental and theoretical frequencies are consistent for the XO_2^+ and XO_3^+ cations. The MP2 calculations provide further support, predicting higher frequencies for the asymmetric XO_2 stretches ($\nu_3(B_2)$) and lower frequencies for the symmetric XO_2 stretches ($\nu_1(A_1)$) when compared with QCISD values. Although the XO_2^+ cations do not have bending modes resembling the out-of-plane bends ($\nu_2(A_2'')$)

(79) Nakamoto, K. *Infrared and Raman Spectra of Inorganic and Coordination Compounds. Part A, Theory and Applications in Inorganic Chemistry*, 5th ed.; Wiley and Sons: New York 1997; p 387.
(80) Bertolini, J. C. *J. Emerg. Med.* **1992**, *10*, 163–168.
(81) Peters, D.; Miethchen, R. *J. Fluorine Chem.* **1996**, *79*, 161–165.

of the XO_3^+ cations, the frequency ranges among the MPW1PW91, B3LYP, MP2, QCISD, and CCSD(T) values for the $\nu_2(A_2'')$ (ClO_3^+, 40 cm^{-1}; BrO_3^+, 49 cm^{-1}) and $\nu_4(E')$ (ClO_3^+, 38 cm^{-1}; BrO_3^+, 15 cm^{-1}) bending modes suggest that they are not strongly dependent on the computational method. The orderings of the calculated frequencies for the XO_3^+ cations are in agreement with those of other trigonal planar AX_3 species.[79]

Conclusion

The fluoride ion donor behaviors of BrO_3F and ClO_3F toward the strong fluoride ion acceptors, AsF_5 and SbF_5, have been investigated. The inability to isolate salts containing the BrO_3^+ or ClO_3^+ cations is in qualitative agreement with the positive values of $\Delta G°$ estimated for these reactions and is strongly related to the high enthalpy of fluoride ion detachment from the parent perhalyl fluorides (ca. 1000 kJ mol^{-1}). The spontaneous reaction of BrO_3F with liquid SbF_5 or SbF_5 dissolved in AsF_5 to form $[BrO_2][Sb_nF_{5n+1}]$ contrasts with the inertness of ClO_3F toward liquid SbF_5. Although estimates of $\Delta G°$ for the reactions of BrO_3F and ClO_3F with SbF_5 to form the $[XO_2][SbF_6]$ salts with the evolution of O_2 indicate both reactions are spontaneous, the reaction involving BrO_3F is 50−54 kJ mol^{-1} more exothermic than for ClO_3F. Comparisons of $\Delta G°$ for reactions involving $(SbF_5)_n$ ($n = 1-3$) and the observation that BrO_3F only reacts with polymeric, liquid SbF_5 suggest that the contrasting reactivities of BrO_3F and ClO_3F are kinetic in origin. The study has also made available fluoride ion affinities for AsF_5 and $(SbF_5)_n$ ($n = 1-3$) up to and including the CCSD(T) level of theory.

The X-ray crystal structures of $[BrO_2][SbF_6]$ and $[ClO_2][SbF_6]$ were determined, with the former providing the first crystallographic characterization of BrO_2^+. The earlier theoretical analyses of the structure and vibrational frequencies of BrO_2^+ have been extended to include the HF, MPW1PW91, B3LYP, and CCSD(T) methods, and the modeling of the geometry and vibrational spectra of ClO_2^+ has been accomplished by use of the HF, MPW1PW91, B3LYP, MP2, QCISD, and CCSD(T) methods. Of these methods, the DFT functional, B3LYP, and the QCISD and CCSD(T) calculations provided the most reliable correlations with the experimental structures and vibrational frequencies of BrO_2^+ and ClO_2^+ and likely provide reliable estimates of the geometric parameters and vibrational frequencies of BrO_3^+ and ClO_3^+, as well as benchmarks for calculations involving chlorine and bromine fluoride and oxide fluoride species.

Experimental Section

Caution! *Anhydrous HF must be handled using appropriate protective gear with immediate access to proper treatment procedures*[80–82] *in the event of contact with liquid aHF or HF vapor. Perbromyl fluoride, ClO_3F, ClO_2F and the salts of ClO_2^+ and BrO_2^+ are strong oxidants and may react vigorously to explosively with water, organic and other oxidizable materials.*

Apparatus and Materials. Volatile materials were handled using vacuum lines constructed of nickel, stainless steel, and hexafluoropropylene-tetrafluoroethylene copolymer (FEP), whereas nonvolatile materials were handled in the inert atmosphere of a drybox.[83] All preparative work was carried out in previously dried and fluorine passivated $^1/_4$-in. o.d. FEP reaction vessels equipped with 316 stainless steel Whitey ORM2 valves, whereas crystal growth was carried out in similar vessels which had a second $^1/_4$-in. o.d. length of FEP tubing fused perpendicular to it about $^1/_3$ of the distance from the valve to give a T-shaped reaction vessel. Samples were stored in valved FEP vessels at −78 °C under dry Ar or N_2.

Potassium perbromate,[84] SbF_5, and AsF_5[85] were prepared and purified according to literature methods. Anhydrous HF was purified as previously described[86] and stored over BiF_5 in a Kel-F vessel. Perbromyl fluoride[26,34,42] and ClO_2F[87] were prepared as previously described. Perchloryl fluoride (Pennwalt Chemicals Corp.) was used without further purification.

Attempted Syntheses of $[BrO_3][Sb_nF_{5n+1}]$ ($n \geq 1$); Synthesis and Purification of $[BrO_2][SbF_6]$. The synthesis of $[BrO_3][Sb_nF_{5n+1}]$ was attempted by the reaction of BrO_3F with excess SbF_5 (eq 3). In a typical experiment, BrO_3F (0.55 mmol) was prepared in situ and condensed into a Y-shaped FEP vessel containing a large excess of liquid SbF_5 (ca. 0.5 mL, 7 mmol), which had been previously distilled into the vessel under dynamic vacuum. The vessel was backfilled with argon, and the reagents were warmed to 0 °C in an ice bath. Perbromyl fluoride reacted vigorously at the SbF_5 surface with the evolution of oxygen, producing a red-orange solid. The Raman spectrum (−110 °C) of the product exhibited two intense Br−O stretches at 870 and 937 cm^{-1}, which were similar to those reported for $[BrO_2][Sb_{2.24}F_{12.2}]$ (865, 932 cm^{-1}).[24] Excess SbF_5 was removed under dynamic vacuum at ambient temperature, and the contents of the reaction vessel were transferred to a T-shaped FEP vessel, followed by the addition of aHF (0.5 mL). The salt, $[BrO_2][SbF_6]$, was isolated in high purity by slowly cooling the pale orange solution from 0 to −70 °C over a period of several hours and by decanting the supernatant into the sidearm of the vessel, which had been precooled to −196 °C. The block-shaped, red-orange colored crystals were dried under dynamic vacuum, and the sidearm of the vessel was heat-sealed off prior to backfilling the vessel with dry nitrogen. The product was identified as $[BrO_2][SbF_6]$ by Raman spectroscopy and single crystal X-ray diffraction.

Because the BrO_3^+ cation may be unstable at temperatures above 0 °C, the abstraction of fluoride from BrO_3F was also attempted at lower temperatures using SbF_5 dissolved in AsF_5 and liquid AsF_5. Perbromyl fluoride did not react with AsF_5 at −78 °C but reacted slowly with SbF_5 dissolved in AsF_5 at −45 °C to produce $[BrO_2][Sb_nF_{5n+1}]$, which was identified by Raman spectroscopy upon removal of AsF_5 under vacuum at −45 °C.

Attempted Synthesis of $[ClO_3][Sb_nF_{5n+1}]$ ($n \geq 1$). The synthesis of $[ClO_3][Sb_nF_{5n+1}]$ was attempted by the reaction of ClO_3F with neat SbF_5. Perchloryl fluoride (2.04 mmol) was condensed into an FEP vessel containing 0.5 mL of neat SbF_5 (ca. 7 mmol). The vessel was backfilled with argon and warmed to ambient temperature overnight. The Raman spectrum of the mixture exhibited an intense ClO_3 stretching band at 1058 cm^{-1}, consistent with that of the

(82) Segal, E. B. *Chem. Health Saf.* **2000**, *7*, 18–23.

(83) Casteel, W. J., Jr.; Kolb, P.; LeBlond, N.; Mercier, H. P. A.; Schrobilgen, G. J. *Inorg. Chem.* **1996**, *35*, 929–942.

(84) Appelman, E. H. *Inorg. Chem.* **1969**, *8*, 223–227.

(85) Emara, A.A. A.; Lehmann, J. F.; Schrobilgen, G. J. *J. Fluorine Chem.* **2005**, *126*, 1373–1376.

(86) Emara, A. A. A.; Schrobilgen, G. J. *Inorg. Chem.* **1992**, *31*, 1323–1332.

(87) Christe, K. O.; Wilson, R. D.; Schack, C. J. *Inorg. Synth.* **1986**, *24*, 3–6.

symmetric ClO_3 stretching band reported for gaseous ClO_3F ($\nu_1(A_1)$, 1063 cm^{-1}).[88] The failure of ClO_3F to react with SbF_5 to form salts containing either the ClO_3^+ or the ClO_2^+ cations was further confirmed by the volatilities of the components of this mixture under dynamic vacuum at ambient temperature.

Synthesis and Purification of $[ClO_2][SbF_6]$. The salt, $[ClO_2][SbF_6]$, was prepared in a $^1/_4$-in. o.d. FEP reaction vessel equipped with a Kel-F valve. Chloryl fluoride (4.16 mmol) was condensed into a vessel containing SbF_5 (3.64 mmol) dissolved in aHF (0.75 mL). The vessel was warmed to ambient temperature for 30 min to allow the reagents to mix and completely react (eq 4) and then cooled to 0 °C, at which temperature the HF solvent and excess ClO_2F were removed under dynamic vacuum. A portion of the crude product (ca. 200 mg) was transferred into a T-shaped FEP vessel and completely dissolved in aHF (1 mL) at ambient temperature. This solution was slowly cooled to −65 °C to recrystallize the $[ClO_2][SbF_6]$ salt. The HF solvent was decanted into the sidearm of the vessel and was subsequently removed under dynamic vacuum at −196 °C. The product was dried under dynamic vacuum at −65 °C and stored under dry nitrogen at −78 °C. No significant impurities were detected in the Raman spectrum (−163 °C) of the pale yellow product.

X-ray Crystallography. (a) Crystal Mounting and Data Collection. Single crystals of $[BrO_2][SbF_6]$ and $[ClO_2][SbF_6]$ were grown as described above and were mounted on a glass fiber using a Fomblin oil as an adhesive at −110 ± 5 °C as previously described.[89] The crystals were centered on a P4 Siemens diffractometer (−173 °C) equipped with a Siemens SMART 1K CCD area detector, a rotating molybdenum anode ($\lambda_{K\alpha}$ = 0.71073 Å, monochromated by a graphite crystal) and controlled by SMART.[90] The distance between the crystal and the detector face was 4.987 cm for $[BrO_2][SbF_6]$ and 5.000 cm for $[ClO_2][SbF_6]$, and the data sets were collected in 512 × 512 pixel mode using 2 × 2 pixel binning. The raw diffraction data sets were integrated in three dimensions using SAINT+,[91] which applied Lorentz and polarization corrections to the integrated intensities. Scaling of the integrated data was performed with SADABS,[92] which applied decay corrections and an empirical absorption correction on the basis of the intensity ratios of redundant reflections.

(b) Solution and Refinement. The program XPREP[93] was used to confirm unit cell dimensions and space groups. Direct methods were used to locate the bromine atoms, and the lighter atom positions were identified in successive difference Fourier syntheses. Final refinements were obtained using data that had been corrected for absorption by introducing an extinction coefficient and were optimized using anisotropic thermal parameters for all atoms.

Raman Spectroscopy. The low-temperature Raman spectra were recorded on a Bruker RFS 100 FT-Raman spectrometer using 1064-nm excitation as previously described.[89]

Computational Details. Structures were optimized using the density functional theory (DFT) level with the MPW1PW91[94] and the B3LYP[95–98] hybrid functionals and at the ab initio levels HF, MP2, and QCISD using the Gaussian 98[95] program package. Single-point energy calculations and optimizations at the coupled-cluster level up to and including CCSD(T) have been performed using the MOLPRO 2006.1[99] program package. Quasirelativistic, energy-adjusted, small-core pseudopotentials (effective-core potentials, ECP) have been used for As,[100] Sb,[100] and Br.[101] The following basis sets have been used: 6−311G(d)[102–104] for MP2, 6311(G)2d for QCISD, DZVP[105] for MPW1PW91, and the aug-cc-pVTZ[106] and aug-cc-pVQZ[106] for B3LYP and CCSD(T). For comparison, the Gaussian-2 theoretical procedure (G2 theory) which is based on ab initio theory and is implemented in the Gaussian 98 program package has also been used.[107] The program GaussView[108] was used to visualize the vibrational displacements that form the basis of the vibrational mode descriptions given in Tables 3, 8, and Supporting Information, Tables S1, S2, and S5.

Stationary points on the potential energy surface were characterized by harmonic vibrational frequency analyses at each level also providing zero-point energy corrections to the thermochemistry. The subsequent single-point energy calculations have been performed on the B3LYP/aug-cc-pVQZ optimized structures using the same basis set.

The importance of nondynamic correlation in coupled-cluster calculations was assessed by computing the T_1-diagnostic.[109,110] In all cases, the values obtained were sufficiently small to suggest the essentially single-reference character of the wave functions. The methodology used here, in particular for B3LYP optimizations, followed by CCSD(T) single-point energy calculations, is well established as a reliable tool for high-oxidation-state redox thermochemistry, for example, Hg and Ir systems.[111,112] Spin−orbit corrections are not considered in this work.

Acknowledgment. We thank the donors of the Petroleum Research Fund, administered by the American Chemical Society, for support of this work under ACS-PRF No. 37128-AC3 (G.J.S.) and the Natural Sciences and Engineering Research Council of Canada for a postgraduate scholarship, McMaster University for a Dalley Fellowship (J.F.L.), and the Deutsche Forschungsgemeinschaft (DFG) for a research fellowship (S.R.). The authors are grateful to Prof. Dr. Martin Kaupp (Institut für Anorganische Chemie der Universität

(88) Claassen, H. H.; Appelman, E. H. *Inorg. Chem.* **1970**, *9*, 622–624.
(89) Gerken, M.; Dixon, D. A.; Schrobilgen, G. J. *Inorg. Chem.* **2000**, *39*, 4244–4255.
(90) *SMART*, release 5.054; Siemens Energy and Automation, Inc.: Madison, WI, 1999.
(91) *SAINT*, release 056.001; Siemens Energy and Automation, Inc.: Madison, WI, 1999.
(92) *SADABS, Siemens Area Detector Absorption Corrections*, version 2.03; Siemens Analytical X-ray Instruments, Inc.: Madison, WI, 1999.
(93) *SHELXTL-Plus*, release 5.1; Siemens Analytical X-ray Instruments, Inc.: Madison, WI, 1998.
(94) Adamo, C.; Barone, V. *J. Chem. Phys.* **1998**, *108*, 664–675.
(95) Frisch, M. J.; et al. *Gaussian 98*; Gaussian.com: Pittsburgh, PA, 1998.
(96) Becke, A. D. *J. Chem. Phys.* **1993**, *98*, 5648–5652.
(97) Lee, C.; Yang, W.; Parr, R. G. *Phys. Rev. B* **1988**, *37*, 785–789.
(98) Miehlich, B.; Savin, A.; Stoll, H.; Preuss, H. *Chem.Phys.Lett.* **1989**, *157*, 200–206.
(99) Werner, H.-J.; et al. *MOLPRO 2006.1, a package of ab initio programs, MOLPRO 2006.1*; Birmingham, U.K., 2006.
(100) Metz, B.; Stoll, H.; Dolg, M. *J. Chem. Phys.* **2000**, *113*, 2563–2569.
(101) Peterson, K. A.; Figgen, D.; Goll, E.; Stoll, H.; Dolg, M. *J. Chem. Phys.* **2003**, *119*, 11113–11123.
(102) McLean, A. D.; Chandler, G. S. *J. Chem. Phys.* **1980**, *72*, 5639–5648.
(103) Krishnan, R.; Binkley, J. S.; Seeger, R.; Pople, J. A. *J. Chem. Phys.* **1980**, *72*, 650–654.
(104) Binning, R. C., Jr.; Curtiss, L. A. *J. Comput. Chem.* **1990**, *11*, 1206–1216.
(105) Godbout, N.; Salahub, D. R.; Andzelm, J.; Wimmer, E. *Can. J. Chem.* **1992**, *70*, 560–571.
(106) Dunning, T. H., Jr *J. Chem. Phys.* **1989**, *90*, 1007–1023.
(107) Curtiss, L. A.; Raghavachari, K.; Trucks, G. W.; Pople, J. A. *J. Chem. Phys.* **1991**, *94*, 7221–7230.
(108) *GaussView*, release 3.0; Gaussian Inc.: Pittsburgh, PA, 2003.
(109) Lee, T. J.; Taylor, P. R. *Int. J. Quantum Chem.* **1989**, *23*, 199–207.
(110) Lee, T. J.; Rice, J. E.; Scuseria, G. E.; Schaefer, H. F., III *Theor. Chim. Acta* **1989**, *75*, 81–98.
(111) Riedel, S.; Straka, M.; Kaupp, M. *Phys. Chem. Chem. Phys.* **2004**, *6*, 1122–1127.
(112) Riedel, S.; Kaupp, M. *Angew. Chem., Int. Ed.* **2006**, *45*, 3708–3711; *Angew. Chem.* **2006**, *118*, 3791−3794.

Würzburg, Germany) for providing computational resources and to Dr. Hélène P.A. Mercier for her critique of the manuscript.

Supporting Information Available: Vibrational frequencies for BrO_2^+ salts (Table S1); vibrational frequencies for ClO_2^+ salts (Table S2); factor-group analyses for $[XO_2][SbF_6]$ (X = Br, Cl) (Table S3); calculated geometries and vibrational frequencies of the $O_2X^+—F\text{-}SbF_5^-$ (*X* = Br, Cl) ion pairs (discussion, Tables S4 and S5); calculated bond length and bond angles for XO_3^+ and XO_2^+ (*X* = Cl, Br) (Table S6); calculated vibrational frequencies of BrO_2^+ and ClO_2^+ (Table S7); complete references 95 (Gaussian 98) and 99 (MOLPRO 2006); and the X-ray crystallographic files (CIF format) for the structure determinations of $[BrO_2][SbF_6]$ and $[ClO_2][SbF_6]$. This material is available free of charge via the Internet at http://pubs.acs.org.

IC800929H